Monthly Notices of the ROYAL ASTRONOMICAL SOCIETY

MNRAS **00,** 1 (2021) https://doi.org/10.1093/mnras/stab2525

A high-resolution line list for AlO

Charles A. Bowesman, Meiyin Shuai, Sergei N. Yurchenko and Jonathan Tennyson ★

Department of Physics and Astronomy, University College London, Gower Street, London WC1E 6BT, UK

Accepted 2021 August 27. Received 2021 August 27; in original form 2021 March 9

ABSTRACT

Indications of aluminium monoxide in atmospheres of exoplanets are being reported. Studies using high-resolution spectroscopy should allow a strong detection but require high-accuracy laboratory data. A MARVEL (measured active rotational-vibrational energy levels) analysis is performed for the available spectroscopic data on $^{27}Al^{16}O$: 22 473 validated transitions are used to determine 6485 distinct energy levels. These empirical energy levels are used to provide an improved, spectroscopically accurate version of the ExoMol ATP line list for $^{27}Al^{16}O$; at the same time, the accuracy of the line lists for the isotopically substituted species $^{26}Al^{16}O$, $^{27}Al^{17}O$, and $^{27}Al^{18}O$ is improved by correcting levels in line with the corrections used for $^{27}Al^{16}O$. These line lists are available from the ExoMol data base at www.exomol.com.

Key words: molecular data – opacity – planets and satellites: atmospheres – stars: atmospheres – ISM: molecules.

1 INTRODUCTION

Aluminium monoxide ($^{27}Al^{16}O$) is a well-known species in cool (Kaminski, Schmidt & Menten 2013) and variable (Banerjee et al. 2003; Tylenda et al. 2005; Banerjee et al. 2012; Kaminski et al. 2016) stars through its electronic spectrum. It has also been observed in Sunspots (Sriramachandran, Viswanathan & Shanmugavel 2013) as well as the winds from oxygen-rich AGB stars (De Beck et al. 2017; Danilovich et al. 2020) and stellar envelopes (Tenenbaum & Ziurys 2009). The radioactive isotope ^{26}Al has a half-life of 70 000 yr so observations of $^{26}Al^{16}O$ have the potential to give timing information but have so far only provided upper limits (Banerjee et al. 2004).

Recently, much attention has turned to the characterization of exoplanet atmospheres. The probable signature of AlO has been observed in the optical transmission spectra of the hot Jupiter exoplanets WASP-33 b (von Essen et al. 2019) and WASP-43b (Chubb et al. 2020c), and more tentatively in hot Jupiter HAT-P-41b (Lewis et al. 2020; Sheppard et al. 2021), and sub-Saturn KELT-11b (Colon et al. 2020). AlO is also thought to be important for temperature inversion in hot Jupiters (Gandhi & Madhusudhan 2019).

The electronic spectrum of AlO is also important for various practical application including studies of laser ablation of aluminium in air (Bol'shakov, Mao & Russo 2017; Ran, Hou & Luo 2017; Van Woerkom et al. 2018), emission in laser-induced plasmas (Surmick & Parigger 2014), explosions (Kimblin et al. 2017), flames (Soo et al. 2017), and emissions from solid fuel rocket exhausts (Knecht et al. 1996). Line lists were provided by Parigger & Hornkohl (2011) for such plasma studies and by Launila & Banerjee (2009) for much cooler mediums; both have the disadvantage from an astronomical perspective of only providing relative intensities. Further recent work has been done to characterize the vibrational and electronic structures of AlO (Honjou 2010, 2014) and to calculate band strengths (Honjou 2011, 2015), radiative lifetimes, and transition probabilities (Feng & Zhu 2019).

Patrascu, Tennyson & Yurchenko (2015) provided AlO line lists covering the four main isotopologues of aluminium monoxide ($^{27}Al^{16}O$, $^{26}Al^{16}O$, $^{27}Al^{17}O$, $^{27}Al^{18}O$) as part of the ExoMol project (Tennyson & Yurchenko 2012). This line list, hereafter referred to as the ATP line list (from the initials of this paper's first author), was based on potential energy and dipole moment curves provided by *ab initio* electronic structure calculations (Patrascu et al. 2014) and variational nuclear motion calculations provided by the then newly developed code DUO (Yurchenko et al. 2016). Many of the studies cited above used the ATP line list.

High-resolution Doppler shift spectroscopy (Birkby 2018) is the most promising method of making a secure detection of exoplanetary AlO. However, although DUO was used to improve the accuracy of the predicted line positions by fitting the potential curves to spectroscopic data, most of the ATP line lists are not of spectroscopic accuracy. In this work, we re-factor the ATP line lists by replacing the calculated energy levels, and hence line positions, with ones derived from empirically determined energy levels. As a result, the majority of the strong lines given by these line lists are predicted with the accuracy of high-resolution spectroscopy making them suitable for studies using high-resolution Doppler shift spectroscopy. An example spectrum generated using the updated line list for $^{27}Al^{16}O$ is shown in Fig. 1 and a breakdown of the empirically determined energy levels is given in Fig. 2.

2 METHOD

Four techniques were employed to give improved energy levels and hence line positions. The backbone of this relies on the MARVEL (measured active rotational-vibrational energy levels) technique (Furtenbacher, Császár & Tennyson 2007) that inverts measured high-resolution spectra to give a set of empirical energy levels and associated uncertainties. All of the measured transitions that were passed through the MARVEL procedure in this work are from the

★ E-mail: j.tennyson@ucl.ac.uk

$^{27}Al^{16}O$ species and these were used to determine these energy levels as part of a spectroscopic network. To ensure continuous coverage and to maximize the connectivity of the network, a few transitions are determined using experimental molecular constants and effective Hamiltonians. The shifts seen in the MARVEL energy levels from their original calculated term values are used to predict the expected changes in the energies of levels in the same regime as but missing from the spectroscopic network. Finally, the energy levels for the three other isotopologues covered in the ATP line list are improved by determining so-called pseudo-experimental energy levels using the technique of Polyansky et al. (2017).

To adapt ExoMol line lists such as ATP for use in high-resolution studies, the ExoMol project has changed its data model to include uncertainties in the energy levels as part of the states file (Tennyson et al. 2020). These uncertainties can then be used to determine the uncertainties in the transition wavenumbers. As the published ATP line list did not contain uncertainties, it is necessary for us to determine these for all the energies given in the states file. How uncertainties are determined is dependent on the technique used to update their energies; each of these techniques is described below.

2.1 MARVEL overview

The MARVEL procedure constructs a graph or network from an input list of transitions, where the nodes of the graph are the energy levels and the edges are the transitions between them; hence the network is known as a spectroscopic network (Császár, Furtenbacher & Árendás 2016). This process allows for observations from multiple sources to be combined into a single, consistent data set. When compiling the input data, each level involved in a transition is required to have a complete set of quantum numbers assigned to it and for consistency the chosen quantum numbers must be the same for all levels. As such, transitions from all sources were updated to define their energy levels using the same set of assignments: their electronic state label, the vibrational quantum number v, the total angular momentum quantum number J, the total angular momentum excluding electronic and nuclear spin N, the fine structure (F_1/F_2), and total parity (+/−). Note that this labelling scheme is based on a Hund's case b coupling scheme while the ATP line list uses Hund's case a that replaces N and F_1/F_2 with Ω (Brown & Carrington 2003). Some of these quantum numbers are redundant, as they are implied by the choice of others (i.e.: the combination of J and N implies the fine structure) but were included to confirm that all assignments had been updated correctly and consistently.

Each transition is identified by a tag that indicates the source paper that the transitions came from and contains a counting number that uniquely identifies each transition within that source. Input transition frequencies require an assigned uncertainty to check the consistency of multiple transitions that connect to the same energy level (Tóbiás et al. 2019). MARVEL determines an optimal uncertainty for each transition, that is the uncertainty required for the transitions to be consistent with the rest of the network. Input transitions are considered inconsistent with the network and are hence invalidated if their optimal uncertainty is greater than the threshold value of 0.05 cm^{-1} and greater than their input uncertainty (transitions input with an uncertainty of 0.1 cm^{-1} are not immediately invalidated). Invalidated transitions remain in the MARVEL transitions file but have a '−' prepended to their frequency value and are thereafter ignored by the MARVEL procedure. These transitions were invalidated in batches when finalizing this new network, starting with those with the highest optimal uncertainties, and the MARVEL procedure was rerun between each batch.

Uncertainties are determined for the individual level energies of the final, self-consistent network by convolving the input uncertainties of all transitions that connect to a given level. MARVEL Online Version 2.1 (Furtenbacher 2020) was used to produce the spectroscopic networks in this study.

2.2 Effective Hamiltonians

The program PGOPHER (Western 2017) was used to solve effective Hamiltonian calculations to obtain transitions that connected otherwise disconnected components of the MARVEL network that contained low-lying energy levels in the X $^2\Sigma^+$ state to the main component of the network. These transitions were calculated using molecular parameters published by Launila & Berg (2011), determined through fits to observed A $^2\Pi_i$–X $^2\Sigma^+$ and B $^2\Sigma^+$–X $^2\Sigma^+$ transitions. Their work only provides updated parameters for the X $^2\Sigma^+$ and B $^2\Sigma^+$ states however and other published constants for the A $^2\Pi_i$ state were not sufficient to reproduce observed transitions to a comparable accuracy. Fortunately, most of the disconnected components of the network containing low-J levels could be connected to the main component, each using a single R- or Q-branch rotational transition, though one component would have required multiple transitions to join up and as such was left out. It was identified that the lowest energy level in our network was not the lowest energy state possible: while we had transitions to the X $^2\Sigma^+$ $v = 0$, $J = 0.5$ f state, the lower energy e state was missing. Hence, another transition was added to this lower state to ensure the correct state was assigned the zero energy value, relative to which all other energy term values are measured.

In total, seven effective Hamiltonian transitions were added to the MARVEL network to ensure that as many of low-lying energy levels of the X $^2\Sigma^+$ state, which are usually determined to a very high accuracy, were connected to the main component of the spectroscopic network. These transitions were assigned an uncertainty of 0.02 cm^{-1} based on the accuracy to which the molecular constants are quoted in their source paper. An exception to this is the single rotational transitions in the X $^2\Sigma^+$ (0,0) band that was added to connect to the lowest energy level in the system, which was assigned an uncertainty of 0.000 001 cm^{-1}. This was done to ensure the lowest energy levels of the network are provided to a high accuracy and also assumes that the blanket uncertainties of 0.0097 and 0.022 cm^{-1}, which was used for all A $^2\Pi_i$–X $^2\Sigma^+$ and B $^2\Sigma^+$–X $^2\Sigma^+$ transitions, respectively, were overestimations in this low-J regime. The network remains fully self-consistent if all effective Hamiltonians are provided with the same uncertainty of 0.000 001 cm^{-1} however, though the other transitions were left with their more conservative estimates. The addition of these effective Hamiltonian transitions did not appear to significantly affect the MARVEL procedure's determination of uncertainties for the other, observed components of the network, suggesting our uncertainty assignments were appropriate.

We produced further effective Hamiltonian transitions in an attempt to extend the network to other missing, low-lying energy levels in the same quantum number regime as the spectroscopic network. After passing these through the MARVEL procedure, however, the final resulting energy term values for these levels had uncertainties determined for them greater than those expected for the initial DUO calculations. As such, these additional transitions were not included in the final network.

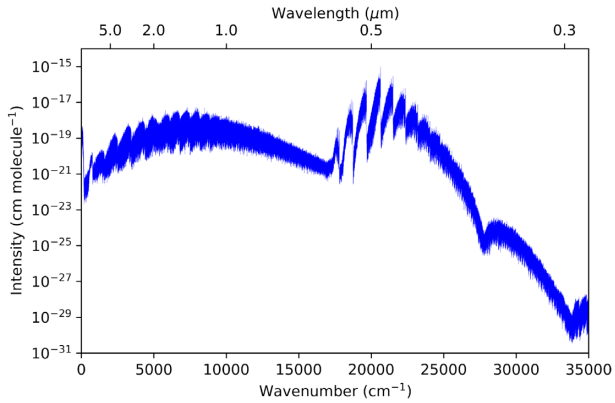

Figure 1. Absorption spectra of ^{27}Al^{16}O at 2000 K computed from the newly updated MARVELized line lists using the code EXOCROSS. Lines have a Voigt profile using broadening parameters taken from Chubb et al. (2020a).

2.3 Hyperfine transitions

While most published observational data do not resolve hyperfine splitting in AlO, Törring & Herrmann (1989), Yamada et al. (1990), and Goto et al. (1994) provide measurements of hyperfine resolved, pure rotational transitions in the ground state. In order to preserve a consistent set of quantum number assignments across all transitions, hyperfine transitions between the same upper and lower energy levels were 'unresolved' into a single line. This was done by calculating a weighted mean line centre, where each transition is weighted by its relative intensity. Measured transition intensities are not provided by these sources so approximate, proportional intensities were calculated using equation (1), adapted from equation (5.174) in Brown & Carrington (2003):

$$I(F', F'', J'', J', I) \propto (2F'+1)(2F''+1)\left\{ \begin{array}{ccc} F' & F'' & 1 \\ J'' & J' & I \end{array} \right\}^2. \qquad (1)$$

Line centres ascertained through this method were assigned uncertainties 10 times greater than those of their constituent hyperfine transitions. A breakdown and analysis of the full treatment for propagating combined hyperfine transition uncertainties will be presented elsewhere.

2.4 Predicted energy shifts

The observationally determined MARVEL levels for ^{27}Al^{16}O show distinct trends in energy shifts from the calculated DUO energies of the original ATP line list. We use these obs. – calc. differences to predict the expected energy shifts from the calculated energy term values of levels missing from the network. These predictions were applied to levels of the same isotopologue in three different ways, depending on whether the levels were in the same quantum number regime as the MARVEL network or not.

First, for levels that did not have a matching entry in the MARVEL network but the equivalently assigned, opposite parity level did have a match, the same energy shift was applied to the unmatched level. The same uncertainty was also applied to these levels as their opposite parity counterpart. This was done to preserve the magnitude of the parity splittings in the DUO levels.

Secondly, the general trends in the obs. – calc. energy shifts seen between the matching MARVEL and DUO energies could be used to predict the energy shifts for any calculated levels that were not updated directly with MARVEL energies, provided these levels had J assignments below the maximum J occurring in the MARVEL network

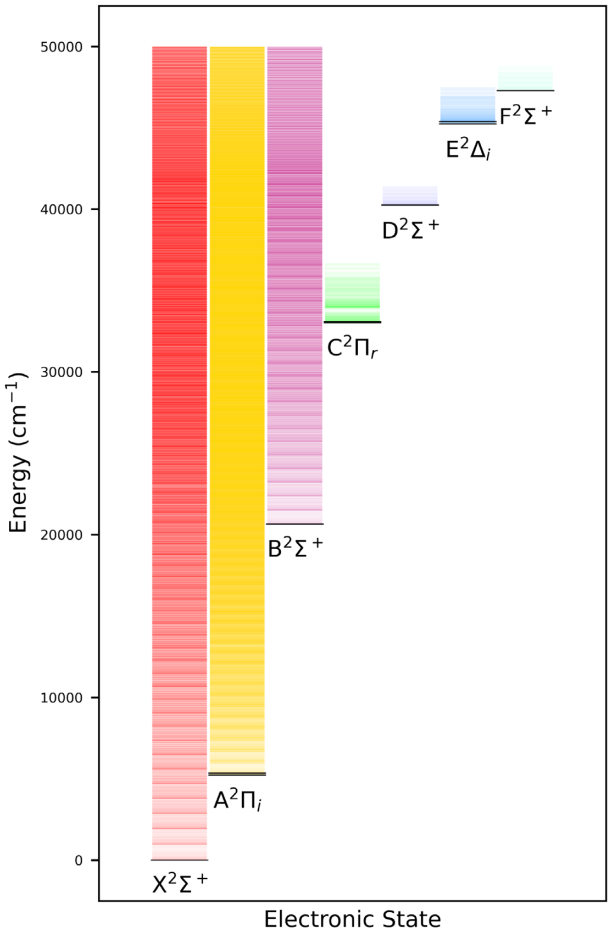

Figure 2. The electronic states of ^{27}Al^{16}O. T_0 values, taken from Launila & Berg (2011), are shown in black while each electronic state's energy levels are marked in a distinct colour. The energy levels shown here are taken from the updated states file produced for this work.

in their respective vibronic band. This energy shift was fit as a function of J for each electronic state, v and Ω configuration for which matching MARVEL/DUO levels existed. Interpolation was used to predict the energy shifts for any missing value of J from $J = 0.5$ up to the maximum value of J contained within the MARVEL network for that band. Any missing J values that were to have their energy shifts predicted were split into groups such that the gaps between the consecutive J values was never more than 10. Huber regression was performed on segments of the data for each of these groups, avoiding fitting all of the data at once and providing predictions that had very low mean-squared errors. The DUO levels corresponding to these missing J levels had their energies corrected by these predicted energy shifts and each took the mean-squared error of their segments regression as their uncertainty. Parity was not considered when interpolating these energy shifts as a parity-dependent shift would not necessarily preserve the original DUO parity splittings. Fig. 3 shows the final energy term values of levels in the X $^2\Sigma^+$, A $^2\Pi_i$, and B $^2\Sigma^+$ states that were updated with MARVEL energies, as well as the levels below the maximum J of each vibrational band that had predicted energy shifts applied to them.

Thirdly, for higher J levels in each vibronic band, the predicted energy shift was taken to be the mean of the obs. – calc. energy shifts of the 10 highest J levels in their respective band and were assigned an initial uncertainty equal to the standard deviation of this value.

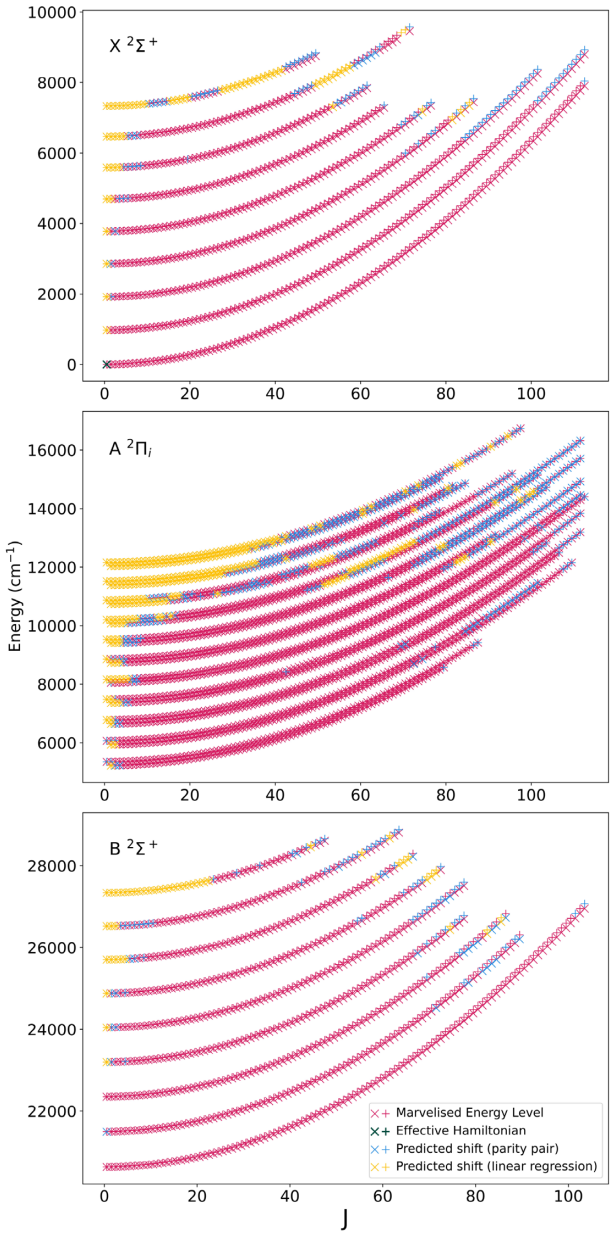

Figure 3. The energy levels of the X $^2\Sigma^+$, A $^2\Pi_i$, and B $^2\Sigma^+$ states of ^{27}Al^{16}O. Levels are coloured based on whether their final energies were determined through MARVEL (pink), effective Hamiltonian calculations (dark green), parity pair correction (blue), or energy shift regression (yellow); e and f parity states are marked with 'x' and ' + ', respectively.

The MARVEL network however has a maximum J of 119.5, whereas the DUO calculations extend up to $J = 300.5$; to account for this extrapolation, the initial uncertainty S is additionally scaled by $J_{\rm ext}$ quadratically, where $J_{\rm ext} = J - J_{\rm max}$ for a given vibronic band:

$$\Delta E_{\rm PE} = S + a J_{\rm ext} (J_{\rm ext} + 1) . \quad (2)$$

The scalefactor a was chosen as 0.0001 cm^{-1} to ensure that any levels with extrapolated energies are consistently less accurate than MARVEL levels. Energy shifts were not extrapolated to higher values of v.

2.5 Pseudo-experimental energy levels

Polyansky et al. (2017) showed for water that the obs. – calc. difference between an empirical energy level obtained using MARVEL and its value given by a variational calculation was almost unchanged on isotopic substitution. They used this method to improve their line lists for $H_2{}^{18}O$ and $H_2{}^{17}O$; the method was recently further refined by Furtenbacher et al. (2020b). This method was used by McKemmish et al. (2019) to provide accurate line lists for several isotopologues of TiO, which led to the identification of features due to four distinct TiO isotopologues in high-resolution spectra of M dwarfs GJ 15A and GJ 15B by Pavlenko et al. (2020).

Here we use the updated – calculated energy differences in ^{27}Al^{16}O, where the updated energies are either the observationally determined MARVEL energies or those with predicted energy shifts, to improve the energy levels of ^{26}Al^{16}O, ^{27}Al^{18}O, and ^{27}Al^{17}O with pseudo-experimental corrections. This ensures that the obs. – calc. energy shifts seen in the MARVEL network are carried over to the equivalently assigned levels in the other AlO isotopologues, as well as the predicted shifts that were modelled on these obs. – calc. trends.

If a level in ^{27}Al^{16}O had been updated from its original energy $E_q^{\rm Duo}(27, 16)$, either with MARVEL energies or through pseudo-experimental corrections to a final energy $E_q^{\rm Updated}(27, 16)$, the same final energy shift was applied to the DUO energies $E_q^{\rm Duo}(X, Y)$ of levels with equivalent quantum number assignments in the three isotopologues ^{26}Al^{16}O, ^{27}Al^{18}O, and ^{27}Al^{17}O:

$$E_q^{\rm PE}(X, Y) = E_q^{\rm Duo}(X, Y) + E_q^{\rm Updated}(27, 16) - E_q^{\rm Duo}(27, 16) . \quad (3)$$

In equation (3), X and Y are used here to denote the aluminium and oxygen mass numbers of respectively, for the species ^{X}Al^{Y}O that the correction is being applied to and q is used to denote a full, unique set of quantum numbers (state, v, J, N, F_1/F_2, $+/-$) following the assignment scheme described earlier.

2.6 Calculated levels

As no attempt was made to extrapolate pseudo-experimental corrections to higher vibrational bands, the only DUO energy term values left unchanged are those that had vibrational quantum number assignments above the maximum value of v for their respective electronic state in the MARVEL network. Any of these original DUO energies that were not updated in this work had an estimate set for their uncertainty. The uncertainty of these levels was expected to grow with the energy and as such was given a quadratic dependence on J and linear dependence on v:

$$\Delta E_{\rm Ca} = a J (J + 1) + b v. \quad (4)$$

Estimates of the factors for the J and and v terms were made as $a = 0.0001$, as in equation (2), and $b = 0.05$ cm^{-1}, respectively.

We swapped the initial DUO energies of nine pairs of X $^2\Sigma^+$ and A $^2\Pi_i$ levels where there existed equivalent MARVEL levels for one or both levels. These levels originally had obs. – calc. energy differences of the order of 60 cm^{-1} but after swapping energies these differences were reduced to around 0.01 cm^{-1}. This occurred due to crossings between the X $^2\Sigma^+$ $v = 6, 7, 8$ and A $^2\Pi_i$ $v = 1, 23$ states, respectively, giving rise to perturbations that caused issues with the DUO assignments. The DUO assignments of J and parity are rigorous but the labelling of electronic and vibrational state are not and as such levels with swapped assignments such as this can occur for levels with very similar energies. While it is possible that additional crossings exist that could result in swapped state assignments, attempts were only made to correct the DUO assignments for levels within the

Table 1. A summary of all experimental sources considered but not included in this study.

Source	Bands/states	Comments
Goodlett & Innes (1959)	B $^2\Sigma^+$–X $^2\Sigma^+$, C $^2\Pi_r$–X $^2\Sigma^a$	No line measurements provided.
Hébert & Tyte (1964)	B $^2\Sigma^+$–X $^2\Sigma^a$	No line measurements provided.
Tyte & Hébert (1964)	B $^2\Sigma^+$–X $^2\Sigma^a$	No line measurements provided.
Tyte (1964)	C $^2\Pi_r$–B $^2\Sigma^a$	No line measurements provided.
Krishnamachari et al. (1966)	D $^2\Sigma^+$–X $^2\Sigma^a$	No line measurements provided, only band heads and other constants.
Tawde & Korwar (1968)	B $^2\Sigma^+$–X $^2\Sigma^a$	No line measurements provided.
McDonald et al. (1969)	C $^2\Pi_r$–X $^2\Sigma^+$	No line measurements provided, only combination differences.
Singh & Narasimham (1969)	D $^2\Sigma^+$–X $^2\Sigma^a$	No line measurements provided.
Johnson et al. (1972)	B $^2\Sigma^+$–X $^2\Sigma^+$	No line measurements provided.
Tawde & Tulasigeri (1972)	D $^2\Sigma^+$–X $^2\Sigma^a$	No line measurements provided.
Schamps (1973)	A $^2\Pi_i$–X $^2\Sigma^+$, B $^2\Sigma^+$–X $^2\Sigma^+$, C $^2\Pi_r$–X $^2\Sigma^+$, C $^2\Pi_r$–B $^2\Sigma^+$, D $^2\Sigma^+$–X $^2\Sigma^+$, D $^2\Sigma^+$–A $^2\Pi_i$, D $^2\Sigma^+$–B $^2\Sigma^+$, E $^2\Delta_i$–A $^2\Pi_i$	Summary of known spectral bands, no new measurements.
Yoshimine et al. (1973)	X $^2\Sigma^+$–X $^2\Sigma^+$, A $^2\Pi_i$–A $^2\Pi_i$, X $^2\Sigma^+$–A $^2\Pi_i$, B $^2\Sigma^+$–B $^2\Sigma^+$, X $^2\Sigma^+$–B $^2\Sigma^+$	No line measurements provided.
Mahieu et al. (1975)	B $^2\Sigma^+$–X $^2\Sigma^+$, D $^2\Sigma^+$–X $^2\Sigma^+$	No line measurements provided.
Rosenwaks et al. (1975)	A $^2\Pi_i$–X $^2\Sigma^+$, B $^2\Sigma^+$–X $^2\Sigma^+$, C $^2\Pi_r$–X $^2\Sigma^+$	No line measurements provided.
Partridge et al. (1983)	B $^2\Sigma^+$–X $^2\Sigma^+$	No line measurements provided.
Singh & Saksena (1983)	C $^2\Pi_r$–X $^2\Sigma^+$	No line measurements provided.
Coxon & Naxakis (1985)	B $^2\Sigma^+$–X $^2\Sigma^+$	No line measurements provided.
Singh & Saksena (1985)	C $^2\Pi_r$–A $^2\Pi_i$, D $^2\Sigma^+$–A $^2\Pi_i$	No line measurements provided, only graphical data.
Singh et al. (1985)	B $^2\Sigma^+$–X $^2\Sigma^+$	No line measurements provided, only band heads and constants.
Saksena et al. (1989)	B $^2\Sigma^+$–X $^2\Sigma^+$	No line measurements provided, only band heads and constants.
Ito (1994)	A $^2\Pi_i$–X $^2\Sigma^+$	No line measurements provided.
Launila & Jonsson (1994)	A $^2\Pi_i$–X $^2\Sigma^+$	Results included and refitted in Launila & Berg (2011).
Bescós et al. (1995)	B $^2\Sigma^+$–X $^2\Sigma^+$	No line measurements provided.
Sato et al. (1995)	B $^2\Sigma^+$–X $^2\Sigma^+$	No line measurements provided.
Kraus et al. (2002)	B $^2\Sigma^+$–X $^2\Sigma^+$	No line measurements provided.
Saksena et al. (2008)	B $^2\Sigma^+$–X $^2\Sigma^+$	Results included and extended upon in Launila & Berg (2011).
Londhe et al. (2010)	B $^2\Sigma^+$–X $^2\Sigma^+$, C $^2\Pi_r$–X $^2\Sigma^+$, C $^2\Pi_r$–A $^2\Pi_i$	No line measurements, only term values and other constants given.
Sarvan et al. (2011)	C $^2\Pi_r$–X $^2\Sigma^+$	Line measurements provided without quantum number assignments.
Bai & Steimle (2020)	B $^2\Sigma^+$–X $^2\Sigma^+$	Line measurements not applicable? Provide G and F transitions in both lower and upper states.
Londhe & Undre (2020)	B $^2\Sigma^+$–X $^2\Sigma^+$	No line measurements provided, transitions recorded with alternative quantum number assignments.

[a]Bands updated to the modern electronic state designation compared to the original source material.

spectroscopic network. Similarly, a series of equal J, Ω, and parity levels with ascending v in the A $^2\Pi_i$ state had had their v assignment shifted up by 1. This was obvious due to initial obs. – calc. energy differences consistently around 700 cm^{-1} for these levels, roughly the expected spacings between A $^2\Pi_i$ state vibrational bands (Ito 1994) that were reduced to near 0.01 cm^{-1} when v was shifted back down by 1. We identified five instances where this had occurred, the first instance being for $J = 86.5$, $\Omega = 1.5$ e parity levels and then subsequently at higher J, though it is possible that similar v assignments shifts have occurred at even higher J, beyond the limit of the MARVEL levels we have to compare against.

3 EXPERIMENTAL DATA SOURCES

3.1 Overview

The following sources were considered when gathering observational data for this study: Goodlett & Innes (1959), Hébert & Tyte (1964), Tyte & Hébert (1964), Tyte (1964), Krishnamachari, Narasimham & Singh (1966), Tawde & Korwar (1968), McDonald & Innes (1969), McDonald et al. (1969), Singh & Narasimham (1969), Johnson, Capelle & Broida (1972), Tawde & Tulasigeri (1972), Schamps (1973), Singh (1973), Yoshimine, McLean & Liu (1973), Mahieu et al. (1975), Rosenwaks, Steele & Broida (1975), Singh & Saksena

Table 2. The changes in the mean and max uncertainty of the 3478 transitions that had their uncertainties updated to the optimal uncertainty determined by MARVEL, broken down by the source paper that the transitions were taken from.

Source	Count	Updated uncertainty mean/max (cm^{-1})	Original uncertainty mean/max (cm^{-1})
11LaBe	3473	0.022 116/0.049 903	0.012 176/0.022 000
94ToJaBoSi	5	0.032 399/0.048 087	0.006 000/0.006 000

(1981), Singh & Saksena (1982), Partridge et al. (1983), Singh & Saksena (1983), Coxon & Naxakis (1985), Singh & Saksena (1985), Singh, Zope & Krishnamachari (1985), Saksena, Ghodgaonkar & Singh (1989), Törring & Herrmann (1989), Yamada et al. (1990), Goto et al. (1994), Ito (1994), Launila & Jonsson (1994), Towle et al. (1994), Bescós, Morley & Ureña (1995), Sato, Ito & Kuchitsu (1995), Kraus, Saykally & Bondybey (2002), Saksena et al. (2008), Londhe et al. (2010), Launila & Berg (2011), Sarvan et al. (2011), Bai & Steimle (2020), Danilovich et al. (2020), and Londhe & Undre (2020). Of these sources, 31 did not provide observational data so were not included in this study; these sources are detailed in Table 1. The majority of these 31 sources did not provide individual line measurements. Launila & Jonsson (1994) and Saksena et al. (2008) provided line measurements but their data were included in the subsequent release by Launila & Berg (2011) where some lines had been remeasured; these data were only taken from the later source.

Papers such as Tawde & Tulasigeri (1972) and most of those published prior to this used different letter designations for some electronic states (excluding the ground state X) or simply did not assign any. Care was taken to ensure assignments were updated for consistency with later works, as described by Singh (1973).

3.2 MARVELized data sources

The following data sources are included in the new spectroscopic network described in this paper.

69McIn (McDonald & Innes 1969): Observations of transitions in the E–A and D–A bands are reported. No uncertainty was provided for the the line measurements in the original paper so was estimated at 0.3 cm^{-1} based on the magnitude of combination differences. The observations of the previously unrecognized, low-lying A $^2\Pi_i$ state reported here prompted a reallocation of the electronic state labels for AlO; what is now known as B $^2\Sigma^+$ was previously the lowest-lying identified band and referred to as A $^2\Sigma^+$.

73Singh (Singh 1973): Observed transitions in the F–A band are reported, stating the absolute accuracy of the reported wavenumbers to be $\pm$0.1 cm^{-1}. This paper details the electronic states of AlO and how their labelling was been updated from earlier works, following the findings of McDonald & Innes (1969); this labelling system is used in this study and in all subsequent papers discussed here.

81SiSa (Singh & Saksena 1981): E–A band transitions are observed. Unblended lines are reported with an accuracy of 0.05 cm^{-1}, based on their agreement with calculated lines reproduced using constants obtained from fits to their data. This value is taken as the uncertainty for these measurements. Some shoulder measurements, blended, and blurred lines were also included with an estimated uncertainty five times this.

82SiSa (Singh & Saksena 1982): This paper reports a series of C–A band observations obtained through the same experimental method as their earlier work (Singh & Saksena 1981) and as such the uncertainties were handled in the same manner.

89ToHe (Törring & Herrmann 1989): This paper reported 12 hyperfine resolved transitions that were combined into a single line. Uncertainty was estimated at 0.05 cm^{-1} based on the magnitude of the reported obs. – calc. values.

90YaCoFuHi (Yamada et al. 1990): This paper reports 56 pure rotation, hyperfine transitions in the $v = 0$ ground state. These were combined into 14 hyperfine-unresolved lines, with each resultant line combining between one and six hyperfine transitions. The uncertainty was taken as the standard deviation of the fit (35 kHz $\sim 1.17 \times 10^{-6}$ cm^{-1}), which was reported as 'only slightly larger than frequency measurement error' that was itself left out. This uncertainty was increased by a factor of 10 after averaging the hyperfine line centres.

94GoTaYaIt (Goto et al. 1994): This paper reports a series of pure rotational, hyperfine-resolved transitions in the ground state in both the $v = 1$ and 2 bands. For both bands, these hyperfine transitions are unresolved into 10 lines each. Hyperfine transitions that they report as unresolved or not included in their fit were not considered when processing their data. No errors are provided for the observed frequencies but it is stated that they are similar to the standards deviations for each vibrational band's least-squares fit; uncertainties of 29 (9.67×10^{-7} cm^{-1}) and 27 kHz (9.00×10^{-7} cm^{-1}) are hence used for the $v = 1$ and 2 bands, respectively.

94ToJaBoSi (Towle et al. 1994): Observations of transitions in the C–X band are reported with a spectral resolution of 180 MHz (0.006 cm^{-1}). This was taken as the uncertainty for this source's measurements.

11LaBe (Launila & Berg 2011): The largest data source included in this study, reporting 21 661 observed transitions in the A–X and B–X bands (16 342 and 5319, respectively). Any calculated values that are included in the published results for this paper were not included in our data set. The uncertainties for measurements in the A–X and B–X bands were taken as 0.0097 and 0.022 cm^{-1}, respectively. A few pure-rotational X $^2\Sigma^+$–X $^2\Sigma^+$ transitions in high vibrational bands (v = 7, 8) were also included in this source that took the same uncertainty as the A–X transitions. This source provides constants that were used to calculate effective Hamiltonian transition wavenumbers for seven low-J, pure rotational ground state transitions to join up low-lying energy levels in disconnected components of the spectroscopic network.

3.3 The MARVEL network

In total, 23 972 input transitions were accessed by MARVEL when building the network and 1499 of these were not validated after optimal uncertainties were calculated for them that were both greater than their input uncertainty and greater than the threshold uncertainty of 0.05 cm^{-1}. Transitions can fail validation for a number of reasons, such as errors in their measurement or quantum number assignment but are principally invalidated due to their inconsistency with the rest of the network. As these transitions connected very few new levels to the network no attempt was made to correct them, such as by changing their quantum number assignment or predicting them using combination differences, though spot checks were manually done to confirm that the reported values had not been incorrectly digitized where the source material had been scanned. These transitions were removed from the final MARVEL network but left in the input data file with negative wavenumber transition frequencies. The vast majority (81.3 per cent) of invalidated transitions came from Launila & Berg (2011), overwhelmingly in the B–X band (79.4 per cent). Transitions from this source make up a greater proportion of the total input

Table 3. A full breakdown of the experimental data sources used to produce the new MARVELized AlO line lists.

Band	Vib.	J range	V/A	Energy range (cm^{-1})	Unc. mean/max (cm^{-1})
PGOPHER_11LaBe (Launila & Berg 2011)					
$X\,^2\Sigma^+$–$X\,^2\Sigma^+$	0–0	0.5–1.5	1/1	1.2778–1.2778	1.00×10^{-6}/1.00×10^{-6}
$X\,^2\Sigma^+$–$X\,^2\Sigma^+$	3–3	2.5–2.5	1/1	3.7361–3.7361	0.020/0.020
$X\,^2\Sigma^+$–$X\,^2\Sigma^+$	4–4	1.5–2.5	2/2	2.4752–3.6942	0.020/0.020
$X\,^2\Sigma^+$–$X\,^2\Sigma^+$	6–6	4.5–5.5	1/1	6.0201–6.0201	0.020/0.020
$X\,^2\Sigma^+$–$X\,^2\Sigma^+$	7–7	6.5–8.5	2/2	9.5555–10.7476	0.020/0.020
89ToHe (Törring & Herrmann 1989)					
$X\,^2\Sigma^+$–$X\,^2\Sigma^+$	0–0	0.5–2.5	2/2	2.5537–2.5539	0.050/0.050
90YaCoFuHi (Yamada et al. 1990)					
$X\,^2\Sigma^+$–$X\,^2\Sigma^+$	0–0	0.5–10.5	14/14	2.5535–12.7659	1.17×10^{-5}/1.17×10^{-5}
94GoTaYaIt (Goto et al. 1994)					
$X\,^2\Sigma^+$–$X\,^2\Sigma^+$	1–1	3.5–10.5	10/10	6.3262–12.6495	9.70×10^{-6}/9.70×10^{-6}
$X\,^2\Sigma^+$–$X\,^2\Sigma^+$	2–2	3.5–10.5	10/10	6.2678–12.5321	9.00×10^{-6}/9.00×10^{-6}
11LaBe (Launila & Berg 2011)					
$X\,^2\Sigma^+$–$X\,^2\Sigma^+$	7–0	58.5–72.5	36/36	6125–6390	0.011/0.021
$X\,^2\Sigma^+$–$X\,^2\Sigma^+$	8–0	9.5–50.5	53/53	7126–7343	0.011/0.029
$A\,^2\Pi_{1/2}$–$X\,^2\Sigma^+$	0–0	1.5–88.5	522/523	4500–5352	0.012/0.046
$A\,^2\Pi_{1/2}$–$X\,^2\Sigma^+$	0–1	0.5–79.5	546/546	3791–4388	0.011/0.041
$A\,^2\Pi_{1/2}$–$X\,^2\Sigma^+$	0–2	24.5–52.5	44/44	3153–3357	0.012/0.030
$A\,^2\Pi_{1/2}$–$X\,^2\Sigma^+$	1–0	0.5–101.5	651/656	4825–6074	0.012/0.047
$A\,^2\Pi_{1/2}$–$X\,^2\Sigma^+$	1–1	1.5–93.5	612/612	4068–5109	0.011/0.039
$A\,^2\Pi_{1/2}$–$X\,^2\Sigma^+$	1–2	18.5–48.5	34/34	3901–4104	0.012/0.036
$A\,^2\Pi_{1/2}$–$X\,^2\Sigma^+$	2–0	2.5–112.5	725/728	5291–6785	0.011/0.047
$A\,^2\Pi_{1/2}$–$X\,^2\Sigma^+$	2–1	6.5–112.5	500/500	4400–5819	0.011/0.035
$A\,^2\Pi_{1/2}$–$X\,^2\Sigma^+$	2–2	5.5–47.5	33/33	4613–4854	0.014/0.034
$A\,^2\Pi_{1/2}$–$X\,^2\Sigma^+$	2–3	12.5–36.5	33/33	3781–3900	0.012/0.038
$A\,^2\Pi_{1/2}$–$X\,^2\Sigma^+$	3–0	2.5–114.5	709/709	5876–7489	0.011/0.045
$A\,^2\Pi_{1/2}$–$X\,^2\Sigma^+$	3–2	8.5–101.5	339/342	4419–5562	0.012/0.043
$A\,^2\Pi_{1/2}$–$X\,^2\Sigma^+$	3–3	33.5–45.5	9/9	4412–4496	0.013/0.024
$A\,^2\Pi_{1/2}$–$X\,^2\Sigma^+$	4–0	6.5–112.5	597/597	6455–8161	0.011/0.046
$A\,^2\Pi_{1/2}$–$X\,^2\Sigma^+$	4–1	21.5–68.5	127/127	6624–7156	0.011/0.027
$A\,^2\Pi_{1/2}$–$X\,^2\Sigma^+$	4–2	12.5–97.5	340/340	5153–6235	0.013/0.047
$A\,^2\Pi_{1/2}$–$X\,^2\Sigma^+$	5–0	1.5–91.5	454/454	7683–8856	0.012/0.047
$A\,^2\Pi_{1/2}$–$X\,^2\Sigma^+$	5–1	6.5–91.5	414/414	6831–7887	0.011/0.040
$A\,^2\Pi_{1/2}$–$X\,^2\Sigma^+$	5–2	19.5–38.5	9/9	6713–6856	0.012/0.024
$A\,^2\Pi_{1/2}$–$X\,^2\Sigma^+$	5–3	17.5–86.5	101/101	5141–5956	0.012/0.046
$A\,^2\Pi_{1/2}$–$X\,^2\Sigma^+$	6–0	4.5–111.5	327/327	7941–9535	0.012/0.041
$A\,^2\Pi_{1/2}$–$X\,^2\Sigma^+$	6–1	10.5–88.5	378/378	7623–8559	0.011/0.044
$A\,^2\Pi_{1/2}$–$X\,^2\Sigma^+$	6–3	6.5–75.5	124/125	5993–6670	0.012/0.046
$A\,^2\Pi_{1/2}$–$X\,^2\Sigma^+$	7–1	8.5–119.5	262/262	7416–9233	0.011/0.037
$A\,^2\Pi_{1/2}$–$X\,^2\Sigma^+$	7–3	31.5–53.5	15/15	6983–7208	0.011/0.031
$A\,^2\Pi_{1/2}$–$X\,^2\Sigma^+$	8–1	10.5–78.5	88/88	8998–9889	0.010/0.010
$A\,^2\Pi_{1/2}$–$X\,^2\Sigma^+$	9–2	36.5–83.5	131/131	8540–9435	0.012/0.049
$A\,^2\Pi_{1/2}$–$X\,^2\Sigma^+$	10–2	41.5–98.5	46/46	8843–9968	0.010/0.010
$A\,^2\Pi_{3/2}$–$X\,^2\Sigma^+$	0–0	3.5–80.5	450/452	4489–5224	0.012/0.041
$A\,^2\Pi_{3/2}$–$X\,^2\Sigma^+$	0–1	1.5–77.5	470/470	3786–4259	0.010/0.050
$A\,^2\Pi_{3/2}$–$X\,^2\Sigma^+$	0–2	14.5–35.5	37/37	3200–3286	0.011/0.025
$A\,^2\Pi_{3/2}$–$X\,^2\Sigma^+$	1–0	2.5–110.5	719/723	4524–5944	0.012/0.047
$A\,^2\Pi_{3/2}$–$X\,^2\Sigma^+$	1–1	3.5–93.5	565/565	4002–4979	0.011/0.044
$A\,^2\Pi_{3/2}$–$X\,^2\Sigma^+$	1–2	41.5–50.5	12/12	3794–3864	0.014/0.035
$A\,^2\Pi_{3/2}$–$X\,^2\Sigma^+$	2–0	1.5–107.5	721/723	5253–6656	0.011/0.047
$A\,^2\Pi_{3/2}$–$X\,^2\Sigma^+$	2–1	5.5–100.5	512/512	4620–5690	0.011/0.049
$A\,^2\Pi_{3/2}$–$X\,^2\Sigma^+$	2–2	23.5–33.5	11/11	4633–4687	0.013/0.024

Table 3 – *continued*

Band	Vib.	J range	V/A	Energy range (cm^{-1})	Unc. mean/max (cm^{-1})
$A\,^2\Pi_{3/2}$–$X\,^2\Sigma^+$	3–0	3.5–104.5	651/653	5977–7358	0.011/0.047
$A\,^2\Pi_{3/2}$–$X\,^2\Sigma^+$	3–2	7.5–84.5	326/328	4667–5423	0.012/0.049
$A\,^2\Pi_{3/2}$–$X\,^2\Sigma^+$	4–0	1.5–115.5	702/702	6338–8052	0.011/0.048
$A\,^2\Pi_{3/2}$–$X\,^2\Sigma^+$	4–1	19.5–74.5	115/115	6451–7040	0.011/0.034
$A\,^2\Pi_{3/2}$–$X\,^2\Sigma^+$	4–2	2.5–85.5	375/377	5251–6126	0.012/0.046
$A\,^2\Pi_{3/2}$–$X\,^2\Sigma^+$	5–0	4.5–111.5	478/478	7158–8736	0.011/0.043
$A\,^2\Pi_{3/2}$–$X\,^2\Sigma^+$	5–1	5.5–79.5	339/339	6937–7764	0.011/0.034
$A\,^2\Pi_{3/2}$–$X\,^2\Sigma^+$	5–3	14.5–72.5	72/73	5318–5858	0.011/0.030
$A\,^2\Pi_{3/2}$–$X\,^2\Sigma^+$	6–0	3.5–103.5	318/318	8005–9413	0.012/0.046
$A\,^2\Pi_{3/2}$–$X\,^2\Sigma^+$	6–1	7.5–99.5	327/327	7206–8435	0.011/0.050
$A\,^2\Pi_{3/2}$–$X\,^2\Sigma^+$	6–3	10.5–61.5	150/150	6077–6544	0.011/0.048
$A\,^2\Pi_{3/2}$–$X\,^2\Sigma^+$	7–0	43.5–83.5	30/30	9137–9833	0.010/0.012
$A\,^2\Pi_{3/2}$–$X\,^2\Sigma^+$	7–1	4.5–104.5	313/313	7692–9109	0.011/0.037
$A\,^2\Pi_{3/2}$–$X\,^2\Sigma^+$	8–1	15.5–95.5	176/176	8662–9737	0.014/0.041
$A\,^2\Pi_{3/2}$–$X\,^2\Sigma^+$	8–2	32.5–84.5	47/47	7908–8685	0.016/0.038
$A\,^2\Pi_{3/2}$–$X\,^2\Sigma^+$	9–1	51.5–77.5	40/40	9595–10051	0.013/0.039
$A\,^2\Pi_{3/2}$–$X\,^2\Sigma^+$	9–2	27.5–86.5	58/58	8480–9372	0.012/0.033
$A\,^2\Pi_{3/2}$–$X\,^2\Sigma^+$	10–2	33.5–78.5	41/41	9273–9961	0.010/0.010
$B\,^2\Sigma^+$–$X\,^2\Sigma^+$	0–0	0.5–104.5	344/350	20 109–20 645	0.023/0.050
$B\,^2\Sigma^+$–$X\,^2\Sigma^+$	0–1	1.5–78.5	222/227	19 380–19 682	0.023/0.042
$B\,^2\Sigma^+$–$X\,^2\Sigma^+$	0–2	2.5–49.5	69/164	18 602–18 732	0.027/0.047
$B\,^2\Sigma^+$–$X\,^2\Sigma^+$	1–0	1.5–86.5	245/265	21 089–21 507	0.024/0.047
$B\,^2\Sigma^+$–$X\,^2\Sigma^+$	1–1	0.5–90.5	244/261	20 129–20 543	0.023/0.050
$B\,^2\Sigma^+$–$X\,^2\Sigma^+$	1–2	1.5–87.5	116/253	19 291–19 593	0.027/0.050
$B\,^2\Sigma^+$–$X\,^2\Sigma^+$	1–3	0.5–67.5	41/184	18 591–18 655	0.026/0.049
$B\,^2\Sigma^+$–$X\,^2\Sigma^+$	2–0	12.5–55.5	99/143	22 149–22 361	0.026/0.047
$B\,^2\Sigma^+$–$X\,^2\Sigma^+$	2–1	0.5–87.5	187/252	20 973–21 398	0.024/0.050
$B\,^2\Sigma^+$–$X\,^2\Sigma^+$	2–2	3.5–82.5	155/208	20 111–20 448	0.026/0.049
$B\,^2\Sigma^+$–$X\,^2\Sigma^+$	2–3	0.5–86.5	58/216	19 183–19 512	0.025/0.048
$B\,^2\Sigma^+$–$X\,^2\Sigma^+$	2–4	0.5–75.5	173/196	18 364–18 592	0.024/0.044
$B\,^2\Sigma^+$–$X\,^2\Sigma^+$	3–1	2.5–56.5	122/187	22 024–22 245	0.028/0.048
$B\,^2\Sigma^+$–$X\,^2\Sigma^+$	3–2	1.5–78.5	206/218	20 959–21 293	0.024/0.050
$B\,^2\Sigma^+$–$X\,^2\Sigma^+$	3–4	2.5–91.5	201/210	19 170–19 438	0.023/0.049
$B\,^2\Sigma^+$–$X\,^2\Sigma^+$	3–5	1.5–66.5	137/148	18 357–18 533	0.023/0.036
$B\,^2\Sigma^+$–$X\,^2\Sigma^+$	4–2	2.5–62.5	153/189	21 887–22 134	0.024/0.048
$B\,^2\Sigma^+$–$X\,^2\Sigma^+$	4–3	4.5–78.5	89/210	20 872–21 198	0.025/0.049
$B\,^2\Sigma^+$–$X\,^2\Sigma^+$	4–5	1.5–67.5	175/186	19 183–19 371	0.023/0.045
$B\,^2\Sigma^+$–$X\,^2\Sigma^+$	4–6	5.5–58.5	109/112	18 333–18 479	0.023/0.048
$B\,^2\Sigma^+$–$X\,^2\Sigma^+$	5–3	1.5–67.5	79/185	21 778–22 030	0.026/0.049
$B\,^2\Sigma^+$–$X\,^2\Sigma^+$	5–4	8.5–72.5	161/186	20 851–21 108	0.024/0.049
$B\,^2\Sigma^+$–$X\,^2\Sigma^+$	5–6	7.5–61.5	99/112	19 141–19 305	0.022/0.046
$B\,^2\Sigma^+$–$X\,^2\Sigma^+$	5–7	5.5–44.5	78/78	18 332–18 432	0.022/0.035
$B\,^2\Sigma^+$–$X\,^2\Sigma^+$	6–4	8.5–66.5	150/155	21 731–21 935	0.023/0.049
$B\,^2\Sigma^+$–$X\,^2\Sigma^+$	6–5	9.5–70.5	112/113	20 827–21 025	0.024/0.049
$B\,^2\Sigma^+$–$X\,^2\Sigma^+$	6–7	3.5–48.5	67/67	19 141–19 234	0.023/0.043
$B\,^2\Sigma^+$–$X\,^2\Sigma^+$	7–5	6.5–63.5	123/127	21 613–21 842	0.023/0.048
$B\,^2\Sigma^+$–$X\,^2\Sigma^+$	7–6	3.5–50.5	64/66	20 825–20 951	0.023/0.048
$B\,^2\Sigma^+$–$X\,^2\Sigma^+$	8–6	23.5–47.5	50/50	21 631–21 756	0.022/0.026
82SiSa (Singh & Saksena 1982)					
$C\,^2\Pi_{1/2}$–$A\,^2\Pi_{1/2}$	0–1	3.5–41.5	96/123	26 940–27 091	0.108/0.250
$C\,^2\Pi_{1/2}$–$A\,^2\Pi_{1/2}$	1–0	5.5–68.5	209/226	28 514–28 859	0.091/0.250
$C\,^2\Pi_{3/2}$–$A\,^2\Pi_{3/2}$	0–1	3.5–29.5	62/69	27 142–27 235	0.108/0.250
$C\,^2\Pi_{3/2}$–$A\,^2\Pi_{3/2}$	1–0	6.5–56.5	170/182	28 712–28 959	0.092/0.250

Table 3 – *continued*

Band	Vib.	J range	V/A	Energy range (cm^{-1})	Unc. mean/max (cm^{-1})
94ToJaBoSi (Towle et al. 1994)					
$C\ ^2\Pi_{1/2}$–$X\ ^2\Sigma^+$	0–0	0.5–17.5	47/59	32 986–33 030	0.007/0.031
$C\ ^2\Pi_{3/2}$–$X\ ^2\Sigma^+$	0–0	1.5–11.5	27/31	33 062–33 100	0.010/0.048
69McIn (McDonald & Innes 1969)					
$D\ ^2\Sigma^+$–$A\ ^2\Pi_{1/2}$	0–0	9.5–46.5	64/64	34 841–34 923	0.300/0.300
$D\ ^2\Sigma^+$–$A\ ^2\Pi_{3/2}$	0–0	9.5–45.5	78/78	34 950–35 033	0.300/0.300
$E\ ^2\Delta_{3/2}$–$A\ ^2\Pi_{1/2}$	0–0	11.5–35.5	68/110	39 909–39 985	0.300/0.300
$E\ ^2\Delta_{5/2}$–$A\ ^2\Pi_{3/2}$	0–0	11.5–36.5	107/124	39 896–39 980	0.300/0.300
81SiSa (Singh & Saksena 1981)					
$E\ ^2\Delta_{3/2}$–$A\ ^2\Pi_{1/2}$	0–0	8.5–67.5	236/262	397 01–39 985	0.182/0.250
$E\ ^2\Delta_{3/2}$–$A\ ^2\Pi_{1/2}$	0–1	17.5–65.5	188/214	39 051–39 265	0.191/0.250
$E\ ^2\Delta_{5/2}$–$A\ ^2\Pi_{3/2}$	0–0	7.5–60.5	240/288	39 754–39 982	0.179/0.250
$E\ ^2\Delta_{5/2}$–$A\ ^2\Pi_{3/2}$	0–1	8.5–60.5	249/278	39 051–39 263	0.177/0.250
73Singh (Singh 1973)					
$F\ ^2\Sigma^+$–$A\ ^2\Pi_{1/2}$	0–0	16.5–49.5	68/72	41 743–41 863	0.100/0.100
$F\ ^2\Sigma^+$–$A\ ^2\Pi_{3/2}$	0–0	14.5–56.5	79/89	41 850–41 972	0.100/0.100

Notes. The total angular momentum quantum number (J) and energy ranges and mean and maximum uncertainties are provided for the validated transitions for each vibronic band, separated by source. The total number of validated transitions compared to those accessed in the MARVEL input file (V/A) is also provided for each band.

Table 4. Source labels used in the new states files to indicate the methods used to produce each entry.

Source label	Meaning
Ca	Calculated with DUO
Ma	MARVELized energy level
EH	Effective Hamiltonian
PS	Predicted shift
PE	Pseudo-experimental correction

transitions however (90.3 per cent) and as such were validated at a higher rate than the average for all sources. Out of all the sources considered, Towle et al. (1994) had the highest proportion of invalidated transitions (17.8 per cent) followed by McDonald & Innes (1969, 15.7 per cent). None of the hyperfine-unresolved transitions from three source Törring & Herrmann (1989), Yamada et al. (1990), or Goto et al. (1994), nor any of the effective Hamiltonian transitions were invalidated.

For the transitions that have optimal uncertainties determined by the MARVEL procedure as greater than their input observational uncertainty but lower than the threshold uncertainty, the input uncertainty was replaced with the MARVEL optimal uncertainty. This process updated the uncertainties of 3478 transitions and resulted in a fully self-consistent network. Of these transitions with updated uncertainties, 3473 came from the Launila & Berg (2011) data set. This is unsurprising, given this source provides the bulk of the observational data that we consider and is likely a consequence of taking a blanket uncertainty value for each electronic band in the absence of individual transition uncertainties. The change in the mean and maximum uncertainties of the transitions that had their uncertainties updated in this manner are given in Table 2 for all sources that were affected.

Hence, the new spectroscopic network consists of 22 473 validated transitions split into 31 components, the largest of which consists of 22 433 transitions connecting 6485 distinct energy levels. Of these levels, one is uniquely determined by effective Hamiltonian calculations. For the other remaining components of the network, 27 consist of single transitions connecting two levels and the remaining three components consist of two, five, and six transitions. The single-transition components all contain transitions involving levels of $J = 53.5$ or above, except for one that is a single B–X (6,7) $P_2(4.5)$ transition that could not be connected to the main component of the network with a single effective Hamiltonian transition. All of the larger disconnected components involve transitions connecting levels with $J > 112.5$. As such, these disconnected components are not considered further in this work. The self-consistency of the network means that the final derived MARVEL energies can be used to recreate all of the input transitions wavenumbers with their uncertainties, for all transitions comprising the largest component of the network. The mean degree of the nodes in the largest component of the MARVEL network is 6.9, which translates to the average number of transitions that connect to and hence determine each energy level. The standard deviation of this however is 9.5 and is reflective of how the degree of the energy levels in our network ranges from 1 to 58. 12.2 per cent of all energy levels are of degree 1 and are hence defined by only a single transition.

Table 3 breaks down the makeup of the new network by experimental data source and vibronic band. Also given are the mean and maximum uncertainties of each listed band, which are the same in most cases due to source papers only providing blanket uncertainty measurements across all of their data. Deviations from this trend are seen in data from two sources (Singh & Saksena 1981, 1982) due to the significant proportion of blended lines that they report.

4 THE NEW LINE LIST

4.1 States files

The revised states files published alongside this paper are updated to include two new properties. The first is the newly calculated uncertainty, measured in wavenumbers and appearing in the fifth

Table 5. An excerpt from the new states file for $^{27}Al^{16}O$.

i	$\tilde{E}$	g	J	unc	τ	+/−	e/f	State	v	$\|\Lambda\|$	$\|\Sigma\|$	$\|\Omega\|$	Source label
1	0.000 000	12	0.5	0.000 001	inf	+	e	X2SIGMA +	0	0	0.5	0.5	EH
2	965.416 878	12	0.5	0.001 651	3.6193e+01	+	e	X2SIGMA +	1	0	0.5	0.5	PS
3	1916.827 286	12	0.5	0.010 519	9.1761e+00	+	e	X2SIGMA +	2	0	0.5	0.5	PS
4	2854.162 814	12	0.5	0.022 148	4.2147e+00	+	e	X2SIGMA +	3	0	0.5	0.5	PS
5	3777.464 572	12	0.5	0.019 275	2.3874e+00	+	e	X2SIGMA +	4	0	0.5	0.5	PS
6	4686.658 929	12	0.5	0.016 235	1.2041e+00	+	e	X2SIGMA +	5	0	0.5	0.5	PS
7	5346.089 546	12	0.5	0.009 700	2.0501e−04	+	e	A2PI	0	1	0.5	0.5	Ma
8	5581.908 884	12	0.5	0.014 747	4.3685e−02	+	e	X2SIGMA +	6	0	0.5	0.5	PS
9	6067.103 586	12	0.5	0.009 700	1.2544e−04	+	e	A2PI	1	1	0.5	0.5	Ma
10	6463.090 252	12	0.5	0.023 150	1.0436e−02	+	e	X2SIGMA +	7	0	0.5	0.5	PS

Notes. i: state counting number;
$\tilde{E}$: term value (in cm^{-1});
g_{tot}: total state degeneracy;
J: total angular momentum quantum number;
unc: estimated uncertainty of energy level (in cm^{-1});
τ: lifetime (in s^{-1});
+/ −: total parity;
e/f: rotationless parity;
State: electronic term value;
v: vibrational quantum number;
$|\Lambda|$: absolute value of the projection of electronic angular momentum;
$|\Sigma|$: absolute value of the projection of the electronic spin;
$|\Omega|$: absolute value of the projection of the total angular momentum;
Source label: method used to generate term value.

column of each entry. The second is a source label that indicates where the energy value came from, differentiating values that were MARVELized, calculated or otherwise had their energies shifted. This appears in the final column of each entry. Table 4 lists values for this source label that have been used so far: 'Ca' has been used in other ExoMol releases (Al-Derzi et al. 2021) while the labels 'Ma', 'EH', 'PS', and 'PE' are introduced for the first time in this work. Entries in the states files produced for this release are marked as 'EH' only when they are singularly determined by calculated effective Hamiltonian transitions; levels that are determined by both effective Hamiltonian calculations and MARVEL data are marked as 'Ma'.

All states files follow the specification outlined by Tennyson, Hill & Yurchenko (2013) to include an ID, state energy, state degeneracy, and J quantum number as the first four columns. This format is intended for use with programs such as EXOCROSS and PGOPHER, both of which were used throughout this work. The first 10 entries of the new states file for $^{27}Al^{16}O$ are shown in Table 5.

As no entries were removed from the original ATP line list when updating them, the new line list retains the same extensive coverage of rovibronic levels in the $X\,^2\Sigma^+$ (28 845 levels, 30.4 per cent of total), $A\,^2\Pi_i$ (54 585, 57.5 per cent), and $B\,^2\Sigma^+$ (10 781, 11.4 per cent) states. This update extends the line list for $^{27}Al^{16}O$ to the higher, previously absent, electronic states $C\,^2\Pi_r$ (319, 0.34 per cent), $D\,^2\Sigma^+$ (37, 0.04 per cent), $E\,^2\Delta_i$ (224, 0.24 per cent), and $F\,^2\Sigma^+$ (71, 0.07 per cent) that are covered in the MARVEL network. The full ranges for each electronic state in the $^{27}Al^{16}O$ states file are shown in Fig. 2. These additional electronic states were not added to the states files for the three ATP isotopologues $^{26}Al^{16}O$, $^{27}Al^{17}O$, and $^{27}Al^{18}O$.

4.2 Spectra

An example absorption spectra for $^{27}Al^{16}O$ at 2000 K is shown in Fig. 1 for transitions involving the $X\,^2\Sigma^+$, $A\,^2\Pi_i$, and $B\,^2\Sigma^+$ states. Fig. 4 shows how the line centres in the generated spectra of $^{27}Al^{16}O$ have shifted with the newly updated, MARVELized state file in comparison to the previous ATP line list. Both of these spectra were generated using the program EXOCROSS (Yurchenko, Al-Refaie & Tennyson 2018c). The two stick spectra shown in Fig. 4 are taken near the peaks of the A–X and B–X bands. As expected from the magnitude of the energy level corrections applied to the states file, the shifts in line centres are quite small, of the order of 10^{-5}–10^{-6} cm^{-1}. These shifts are sufficiently small that they would require resolving powers on average of 1.2×10^5 (for the X–X band), 7.0×10^5 (A–X), and 1.1×10^6 (B–X) to be observed. The relative line intensities remain essentially unchanged as the trans files have not been updated, keeping the same Einstein A coefficients as the ATP line list but differing slightly due to different partition functions. Fig. 5 shows that the appearance for the X–X, A–X, and B–X bands retain a well-defined vibrational structure and the overall shape remains largely the same as the original ATP spectra (Patrascu et al. 2015).

Beyond their use for detecting AlO in exoplanet atmospheres with Doppler spectroscopy, the new line lists could be used in conjunction with high-resolution spectroscopy as a temperature probe. Near band heads, such as that of the prominent B–X (0–0) band shown in Fig. 6, the spacings between subsequent lines decrease until they appear to double back on themselves, meaning high and low J transitions of the same branch can appear in close proximity to one another. These purely rotational transitions can be used to probe the rotational temperature through comparison between the relative intensities of these lines, utilizing the temperature sensitive Boltzmann distribution of the involved levels' populations. This technique has been applied to observed spectra of CO (Jones et al. 2005) and H_2O (Viti et al. 2008) and could be best employed for AlO on telescopes with good coverage of the visible region where the B–X feature is present.

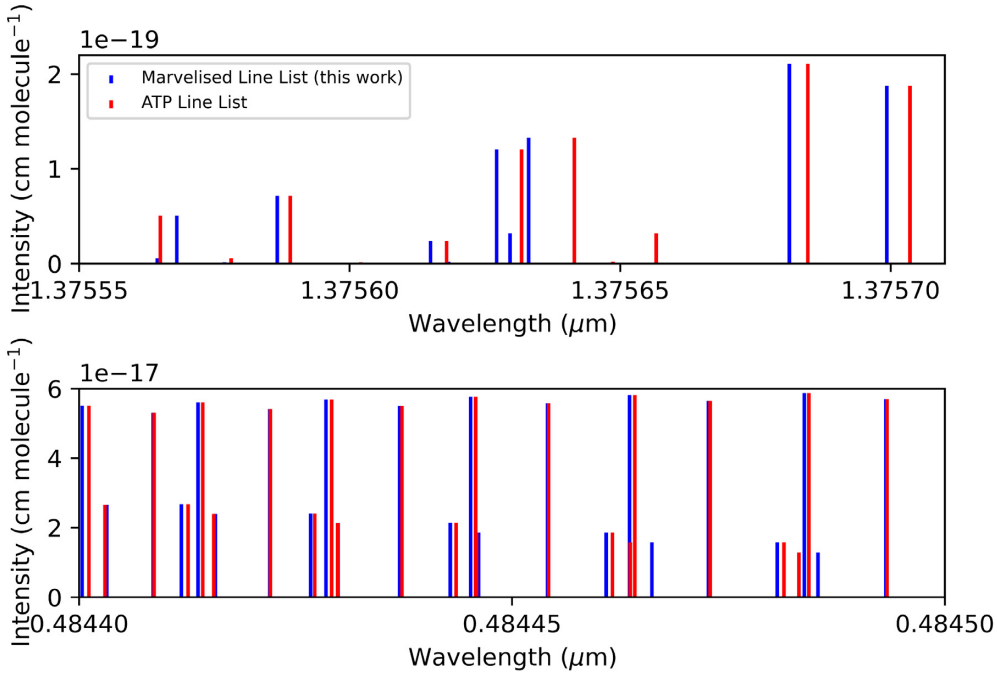

Figure 4. Computed absorption stick spectra at 2000 K from the ATP (Patrascu et al. 2015) and newly updated MARVELized line lists for $^{27}Al^{16}O$, produced using the code EXOCROSS. The top panel is taken from near to peak of the A $^2\Pi_i$–X $^2\Sigma^+$ band and the bottom from near the peak of the B $^2\Sigma^+$–X $^2\Sigma^+$ band.

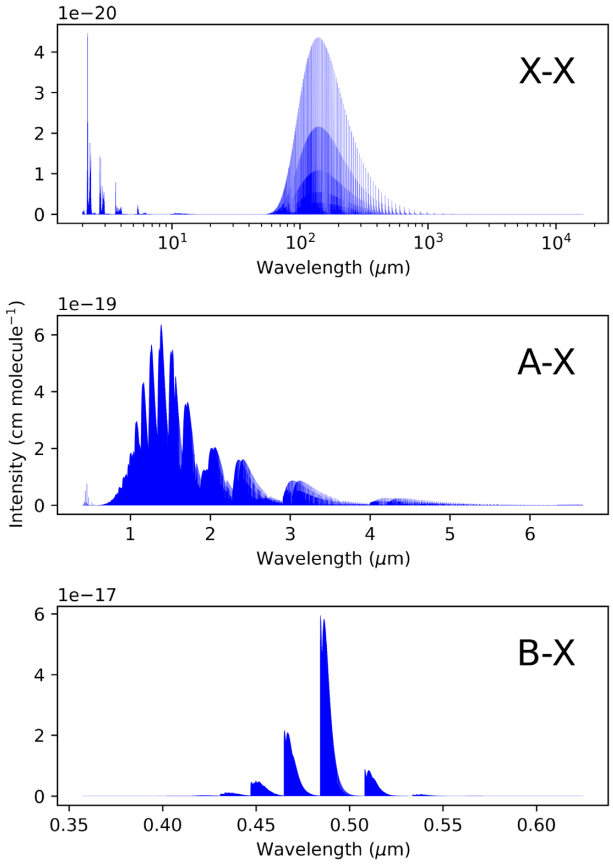

Figure 5. The X $^2\Sigma^+$–X $^2\Sigma^+$, A $^2\Pi_i$–X $^2\Sigma^+$, and B $^2\Sigma^+$–X $^2\Sigma^+$ bands of $^{27}Al^{16}O$ in absorption spectra at 2000 K, computed from the newly MARVELized line list using the code EXOCROSS.

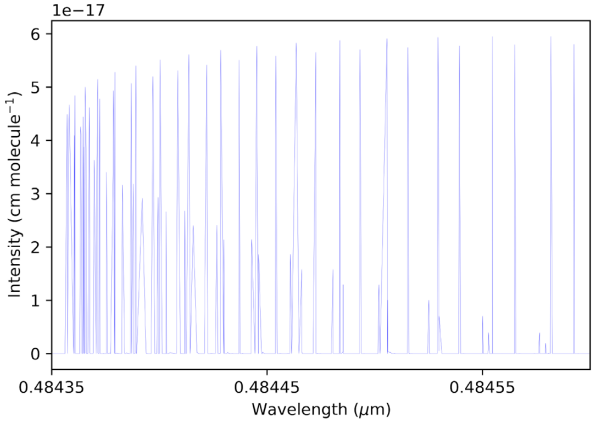

Figure 6. A closeup of the B $^2\Sigma^+$–X $^2\Sigma^+$ (0–0) band head, computed at 2000 K from the newly MARVELized line list using the code EXOCROSS.

5 CONCLUSION

In this paper, we have attempted to compile all appropriate, published experimental data pertaining to AlO into a single, high-resolution data base and comes as part of the continued effort by the ExoMol project to produce new and update existing line lists to this standard (Tennyson et al. 2020). The aim of this is to allow as many transitions as possible to be provided with high-resolution accuracy and, by explicit provision of uncertainties in the individual energies, to allow those transitions that are accurately known to be identified. We are in the process of upgrading the available ExoMol line lists in this fashion. Line lists with energy levels determined by MARVEL and explicit uncertainties are now available for C_2 (Yurchenko et al. 2018b; McKemmish et al. 2020), NH_3 (Coles et al. 2019; Furtenbacher et al. 2020c), C_2H_2 (Chubb et al. 2018; Chubb, Tennyson & Yurchenko 2020b), $H_2{}^{16}O$ (Polyansky et al. 2018; Furtenbacher et al. 2020a), $H_2{}^{17}O$ and $H_2{}^{17}O$ (Polyansky et al. 2017; Furtenbacher et al.

2020b), TiO (McKemmish et al. 2017, 2019), H_2CO (Al-Refaie et al. 2015; Al-Derzi et al. 2021), and AlH (Yurchenko et al. 2018a). The newly constructed XABC line list for NO (Qu, Yurchenko & Tennyson 2021) is the first ExoMol line list made directly in this form. Such a data base of high-resolution line lists is necessary for the thorough classification of molecules in exoplanet spectroscopy and will underpin future studies using techniques such as high-resolution Doppler shift spectroscopy.

The newly added electronic states ($C\ ^2\Pi_r$, $D\ ^2\Sigma^+$, $E\ ^2\Delta_i$, and $F\ ^2\Sigma^+$), comprising 0.7 per cent of the entries in the $^{27}Al^{16}O$ states file, do not currently have any transitions associated with them but these could be calculated if required. The finalized states file for $^{27}Al^{16}O$ consists of 94 862 energy levels, comprising of 1 effective Hamiltonian level, 6484 MARVEL levels, 16 861 predicted energy shift levels, and 71 516 DUO calculated levels. In sum, 73 per cent of MARVEL levels in this states file have an uncertainty lower than 10^{-2} cm^{-1}. The three isotopologues $^{26}Al^{16}O$, $^{27}Al^{17}O$, $^{27}Al^{18}O$ have had no additional levels added to their states files and hence remain the same sizes (93 350, 96 350, and 98 269 levels, respectively), each now comprising of over 16 000 pseudo-experimentally corrected entries.

MARVEL is by construction an active methodology, which means that as new high-resolution data become available, it can straightforwardly be used to produce improved and extended sets of empirical energy levels. As part of the work being undertaken in the ExoMol project, we will update line list whenever new spectroscopic data are published; the goal is to make all line list available as part of an active data base.

ACKNOWLEDGEMENTS

We would like to thank Samuel A. Meek, Tibor Furtebacher, and Atilla G. Császár for discussion on the treatment of hyperfine lines. This work was funded by the European Research Council (ERC) under the European Union's Horizon 2020 research and innovation programme through Advance Grant number 883830 and STFC through grant ST/R000476/1.

DATA AVAILABILITY

The MARVEL transitions and energy files are given as supplementary material. Updated ATP states files for the various isotopologues of AlO can be downloaded from www.exomol.com. Line list metadata are provided in an accompanying `.def` file, including the version number that has been updated to 20210622 as a result of this work.

REFERENCES

Al-Derzi A. R. et al., 2021, J. Quant. Spectrosc. Radiat. Transf., 266, 107563
Al-Refaie A. F., Yurchenko S. N., Yachmenev A., Tennyson J., 2015, MNRAS, 448, 1704
Bai X., Steimle T. C., 2020, ApJ, 889, 147
Banerjee D. P. K., Varricatt W. P., Ashok N. M., Launila O., 2003, ApJ, 598, L31
Banerjee D. P. K., Ashok N. M., Launila O., Davis C. J., Varricatt W. P., 2004, ApJ, 610, L29
Banerjee D. P. K., Varricatt W. P., Mathew B., Launila O., Ashok N. M., 2012, ApJ, 753, L20
Bescós B., Morley G., Ureña A. G., 1995, Chem. Phys. Lett., 244, 407
Birkby J.-L., 2018, preprint (arXiv:e-print)
Bol'shakov A. A., Mao X., Russo R. E., 2017, J. Anal. At. Spectrom., 32, 657
Brown J. M., Carrington A., 2003, Rotational Spectroscopy of Diatomic Molecules. Cambridge Univ. Press, Cambridge
Chubb K. L. et al., 2018, J. Quant. Spectrosc. Radiat. Transf., 204, 42
Chubb K. L. et al., 2020a, A&A, 646, A21
Chubb K. L., Tennyson J., Yurchenko S. N., 2020b, MNRAS, 493, 1531
Chubb K. L., Min M., Kawashima Y., Helling C., Waldmann I., 2020c, A&A, 639, A3
Coles P. A., Yurchenko S. N., Tennyson J., 2019, MNRAS, 490, 4638
Colon K. D. et al., 2020, AJ, 160, 280
Coxon J., Naxakis S., 1985, J. Mol. Spectrosc., 111, 102
Császár A. G., Furtenbacher T., Árendás P., 2016, J. Phys. Chem. A, 120, 8949
Danilovich T. et al., 2020, ApJ, 904, 110
De Beck E., Decin L., Ramstedt S., Olofsson H., Menten K. M., Patel N. A., Vlemmings W. H. T., 2017, A&A, 598, A53
Feng Y., Zhu Z., 2019, J. Quant. Spectrosc. Radiat. Transf., 231, 37
Furtenbacher T., 2020, Marvelonline: MARVEL2.0
Furtenbacher T., Császár A. G., Tennyson J., 2007, J. Mol. Spectrosc., 245, 115
Furtenbacher T., Tóbiás R., Tennyson J., Polyansky O. L., Császár A. G., 2020a, J. Phys. Chem. Ref. Data, 49, 033101
Furtenbacher T., Tóbiás R., Tennyson J., Polyansky O. L., Kyuberis A. A., Ovsyannikov R. I., Zobov N. F., Császár A. G., 2020b, J. Phys. Chem. Ref. Data, 49, 043103
Furtenbacher T., Coles P. A., Tennyson J., Yurchenko S. N., Yu S., Drouin B., Tóbiás R., Császár A. G., 2020c, J. Quant. Spectrosc. Radiat. Transf., 251, 107027
Gandhi S., Madhusudhan N., 2019, MNRAS, 485, 5817
Goodlett V. W., Innes K. K., 1959, Nature, 183, 243
Goto M., Takano S., Yamamoto S., Ito H., Saito S., 1994, Chem. Phys. Lett., 227, 287
Hébert G. R., Tyte D. C., 1964, Proc. Phys. Soc., 83, 629
Honjou N., 2010, J. Mol. Struct., 939, 59
Honjou N., 2011, Comput. Theor. Chem., 978, 138
Honjou N., 2014, Comput. Theor. Chem., 1027, 186
Honjou N., 2015, Comp. Theor. Chem., 1054, 1
Ito H., 1994, Can. J. Phys., 72, 1082
Johnson S. E., Capelle G., Broida H. P., 1972, J. Chem. Phys., 56, 663
Jones H. R. A., Pavlenko Y., Viti S., Barber R. J., Yakovina L., Pinfold D., Tennyson J., 2005, MNRAS, 358, 105
Kaminski T., Schmidt M. R., Menten K. M., 2013, A&A, 549, A6
Kaminski T. et al., 2016, A&A, 592, A42
Kimblin C., Trainham R., Capelle G. A., Mao X., Russo R. E., 2017, Am. Inst. Phys. Adv., 7, 095208
Knecht D. J., Pike C. P., Murad E., Rall D. L. A., 1996, J. Spacecr. Rockets, 33, 677
Kraus D., Saykally R. J., Bondybey V. E., 2002, Chem. Phys. Chem., 3, 364
Krishnamachari S. L. N. G., Narasimham N. A., Singh M., 1966, Can. J. Phys., 44, 2513
Launila O., Banerjee D. P. K., 2009, A&A, 508, 1067
Launila O., Berg L.-E., 2011, J. Mol. Spectrosc., 265, 10
Launila O., Jonsson J., 1994, J. Mol. Spectrosc., 168, 1
Lewis N. K. et al., 2020, ApJ, 902, L19
Londhe C. T., Undre P. B., 2020, J. Phys. Conf. Ser., 1644, 012063
Londhe C. T., Sunanda K., Saksena M. D., Behere S. H., 2010, J. Mol. Spectrosc., 263, 178
McDonald J. K., Innes K. K., 1969, J. Mol. Spectrosc., 32, 501
McDonald J. K., Innes K. K., Goodlett V. W., Tolbert T. W., 1969, J. Mol. Spectrosc., 32, 511
McKemmish L. K. et al., 2017, ApJS, 228, 15
McKemmish L. K., Masseron T., Hoeijmakers J., Pérez-Mesa V. V., Grimm S. L., Yurchenko S. N., Tennyson J., 2019, MNRAS, 488, 2836
McKemmish L. K., Syme A. M., Borsovszky J., Yurchenko S. N., Tennyson J., Furtenbacher T., Csaszar A. G., 2020, MNRAS, 497, 1081
Mahieu J. M., Jacquinot D., Schamps J., Hall J. A., 1975, J. Phys. B: At. Mol. Phys., 8, 308
Parigger C. G., Hornkohl J. O., 2011, Spectra Chim. Acta A, 81, 404
Partridge H., Langhoff S. R., Lengsfield B., Liu B., 1983, J. Quant. Spectrosc. Radiat. Transf., 30, 449

Patrascu A. T., Hill C., Tennyson J., Yurchenko S. N., 2014, J. Chem. Phys., 141, 144312
Patrascu A. T., Tennyson J., Yurchenko S. N., 2015, MNRAS, 449, 3613
Pavlenko Y. V., Yurchenko S. N., McKemmish L. K., Tennyson J., 2020, A&A, 42, A77
Polyansky O. L., Kyuberis A. A., Lodi L., Tennyson J., Ovsyannikov R. I., Zobov N., 2017, MNRAS, 466, 1363
Polyansky O. L., Kyuberis A. A., Zobov N. F., Tennyson J., Yurchenko S. N., Lodi L., 2018, MNRAS, 480, 2597
Qu Q., Yurchenko S. N., Tennyson J., 2021, MNRAS
Ran P., Hou H., Luo S.-N., 2017, J. Anal. At. Spectrom., 32, 2254–2262
Rosenwaks S., Steele R. E., Broida H. P., 1975, J. Chem. Phys., 63, 1963
Saksena M. D., Ghodgaonkar G. S., Singh M., 1989, J. Phys. B: At. Mol. Opt. Phys., 22, 1993
Saksena M. D., Deo M. N., Sunanda K., Behere S. H., Londhe C. T., 2008, J. Mol. Spectrosc., 247, 47
Sarvan M., Perić M., Zeković L., Stojadinović S., Belča I., Petković M., Kasalica B., 2011, Spectra Chim. Acta A, 81, 672
Sato N., Ito H., Kuchitsu K., 1995, Chem. Phys. Lett., 240, 10
Schamps J., 1973, Chem. Phys., 2, 352
Sheppard K. B. et al., 2021, AJ., 161, 51
Singh M., 1973, J. Phys. B: At. Mol. Phys., 6, 521
Singh M., Narasimham N. A., 1969, J. Phys. B: At. Mol. Opt. Phys., 2, 119
Singh M., Saksena M. D., 1981, Can. J. Phys., 59, 955
Singh M., Saksena M. D., 1982, Can. J. Phys., 60, 1730
Singh M., Saksena M. D., 1983, Can. J. Phys., 61, 1347
Singh M., Saksena M. D., 1985, Can. J. Phys., 63, 1162
Singh M., Zope G. V., Krishnamachari S. L. N. G., 1985, J. Phys. B: At. Mol. Phys., 18, 1743
Soo M., Goroshin S., Glumac N., Kumashiro K., Vickery J., Frost D. L., Bergthorson J. M., 2017, Combust. Flame, 180, 230
Sriramachandran P., Viswanathan B., Shanmugavel R., 2013, Solar Phys., 286, 315
Surmick D. M., Parigger C. G., 2014, Appl. Spectrosc., 68, 992
Tawde N. R., Korwar V. M., 1968, J. Phys. B: At. Mol. Phys., 1, 753
Tawde N. R., Tulasigeri V. G., 1972, J. Phys. B: At. Mol. Phys., 5, 1681
Tenenbaum E. D., Ziurys L. M., 2009, ApJ, 694, L59
Tennyson J., Yurchenko S. N., 2012, MNRAS, 425, 21
Tennyson J., Hill C., Yurchenko S. N., Data structures for ExoMol: Molecular line lists for exoplanet and other atmospheres, 2013, AIP Conf. Ser. Vol. 1545, Eighth International Conference on Atomic and Molecular Data and Their Applications, Am. Inst. Phys., New York, p. 186
Tennyson J. et al., 2020, J. Quant. Spectrosc. Radiat. Transf., 255, 107228
Tóbiás R., Furtenbacher T., Tennyson J., Császár A. G., 2019, Phys. Chem. Chem. Phys., 21, 3473
Törring T., Herrmann R., 1989, Mol. Phys., 68, 1379
Towle J., James A., Bourne O., Simard B., 1994, J. Mol. Spectrosc., 163, 300
Tylenda R., Crause L. A., Gorny S. K., Schmidt M. R., 2005, A&A, 439, 651
Tyte D. C., 1964, Nature, 202, 383
Tyte D. C., Hébert G. R., 1964, Proc. Phys. Soc., 84, 830
Van Woerkom T. A., Perram G. P., Dolasinski B. D., Berry P. A., Phelps C. D., 2018, J. Opt. Soc. Am. B, 35, B54
Viti S., Jones H. R. A., Richter M. J., Barber R. J., Tennyson J., Lacy J. H., 2008, MNRAS, 388, 1305
von Essen C., Mallonn M., Welbanks L., Madhusudhan N., Pinhas A., Bouy H., Hansen P. W., 2019, A&A, 622, A71
Western C. M., 2017, J. Quant. Spectrosc. Radiat. Transf., 186, 221
Yamada C., Cohen E. A., Fujitake M., Hirota E., 1990, J. Chem. Phys., 92, 2146
Yoshimine M., McLean A. D., Liu B., 1973, J. Chem. Phys., 58, 4412
Yurchenko S. N., Lodi L., Tennyson J., Stolyarov A. V., 2016, Comput. Phys. Commun., 202, 262
Yurchenko S. N., Williams H., Leyland P. C., Lodi L., Tennyson J., 2018a, MNRAS, 479, 1401
Yurchenko S. N., Szabo I., Pyatenko E., Tennyson J., 2018b, MNRAS, 480, 3397
Yurchenko S. N., Al-Refaie A. F., Tennyson J., 2018c, A&A, 614, A131

SUPPORTING INFORMATION

Supplementary data are available at *MNRAS* online.

Please note: Oxford University Press is not responsible for the content or functionality of any supporting materials supplied by the authors. Any queries (other than missing material) should be directed to the corresponding author for the article.

This paper has been typeset from a TEX/LATEX file prepared by the author.

List of astronomical key words (Updated on 2020 January)

This list is common to *Monthly Notices of the Royal Astronomical Society, Astronomy and Astrophysics*, and *The Astrophysical Journal*. In order to ease the search, the key words are subdivided into broad categories. No more than *six* subcategories altogether should be listed for a paper.

The subcategories in boldface containing the word 'individual' are intended for use with specific astronomical objects; these should never be used alone, but always in combination with the most common names for the astronomical objects in question. Note that each object counts as one subcategory within the allowed limit of six.

The parts of the key words in italics are for reference only and should be omitted when the keywords are entered on the manuscript.

General
editorials, notices
errata, addenda
extraterrestrial intelligence
history and philosophy of astronomy
miscellaneous
obituaries, biographies
publications, bibliography
sociology of astronomy
standards

Physical data and processes
acceleration of particles
accretion, accretion discs
asteroseismology
astrobiology
astrochemistry
astroparticle physics
atomic data
atomic processes
black hole physics
chaos
conduction
convection
dense matter
diffusion
dynamo
elementary particles
equation of state
gravitation
gravitational lensing: micro
gravitational lensing: strong
gravitational lensing: weak
gravitational waves
hydrodynamics
instabilities
line: formation
line: identification
line: profiles
magnetic fields
magnetic reconnection
(magnetohydrodynamics) MHD
masers
molecular data
molecular processes
neutrinos
nuclear reactions, nucleosynthesis, abundances
opacity
plasmas
polarization
radiation: dynamics
radiation mechanisms:general
radiation mechanisms: non-thermal
radiation mechanisms: thermal
radiative transfer
relativistic processes
scattering
shock waves
solid state: refractory
solid state: volatile
turbulence
waves

Astronomical instrumentation, methods and techniques
atmospheric effects
balloons
instrumentation: adaptive optics
instrumentation: detectors
instrumentation: high angular resolution
instrumentation: interferometers
instrumentation: miscellaneous
instrumentation: photometers
instrumentation: polarimeters
instrumentation: spectrographs
light pollution
methods: analytical
methods: data analysis
methods: laboratory: atomic
methods: laboratory: molecular
methods: laboratory: solid state
methods: miscellaneous
methods: numerical
methods: observational
methods: statistical
site testing
space vehicles
space vehicles: instruments
techniques: high angular resolution
techniques: image processing
techniques: imaging spectroscopy
techniques: interferometric
techniques: miscellaneous
techniques: photometric
techniques: polarimetric
techniques: radar astronomy
techniques: radial velocities
techniques: spectroscopic
telescopes

Astronomical data bases
astronomical data bases: miscellaneous
atlases
catalogues
surveys
virtual observatory tools

Software
software: data analysis
software: development
software: documentation
software: public release
software: simulations

Astrometry and celestial mechanics
astrometry
celestial mechanics
eclipses
ephemerides
occultations
parallaxes
proper motions
reference systems
time

The Sun
Sun: abundances
Sun: activity
Sun: atmosphere
Sun: chromosphere
Sun: corona
Sun: coronal mass ejections (CMEs)
Sun: evolution
Sun: faculae, plages
Sun: filaments, prominences
Sun: flares
Sun: fundamental parameters
Sun: general
Sun: granulation
Sun: helioseismology
Sun: heliosphere
Sun: infrared
Sun: interior
Sun: magnetic fields
Sun: oscillations
Sun: particle emission
Sun: photosphere
Sun: radio radiation
Sun: rotation
(Sun:) solar–terrestrial relations
(Sun:) solar wind
(Sun:) sunspots
Sun: transition region
Sun: UV radiation
Sun: X-rays, gamma-rays

Planetary systems
comets: general

comets: individual: . . .
Earth
interplanetary medium
Kuiper belt: general

Kuiper belt objects: individual: . . .
meteorites, meteors, meteoroids
minor planets, asteroids: general
minor planets, asteroids: individual: . . .
Moon
Oort Cloud
planets and satellites: atmospheres
planets and satellites: aurorae
planets and satellites: composition
planets and satellites: detection
planets and satellites: dynamical evolution and stability
planets and satellites: formation
planets and satellites: fundamental parameters
planets and satellites: gaseous planets
planets and satellites: general

planets and satellites: individual: . . .
planets and satellites: interiors
planets and satellites: magnetic fields
planets and satellites: oceans
planets and satellites: physical evolution
planets and satellites: rings
planets and satellites: surfaces
planets and satellites: tectonics
planets and satellites: terrestrial planets
planet–disc interactions
planet–star interactions
protoplanetary discs
zodiacal dust

Stars
stars: abundances
stars: activity
stars: AGB and post-AGB
stars: atmospheres
(stars:) binaries *(including multiple)*: close
(stars:) binaries: eclipsing
(stars:) binaries: general
(stars:) binaries: spectroscopic
(stars:) binaries: symbiotic
(stars:) binaries: visual
stars: black holes
(stars:) blue stragglers
(stars:) brown dwarfs
stars: carbon
stars: chemically peculiar
stars: chromospheres
(stars:) circumstellar matter
stars: coronae
stars: distances
stars: dwarf novae
stars: early-type
stars: emission-line, Be
stars: evolution
stars: flare
stars: formation
stars: fundamental parameters
(stars:) gamma-ray burst: general
(stars:) **gamma-ray burst: individual: . . .**
stars: general
(stars:) Hertzsprung–Russell and colour–magnitude diagrams
stars: horizontal branch
stars: imaging
stars: individual: . . .
stars: interiors

stars: jets
stars: kinematics and dynamics
stars: late-type
stars: low-mass
stars: luminosity function, mass function
stars: magnetars
stars: magnetic field
stars: massive
stars: mass-loss
stars: neutron
(stars:) novae, cataclysmic variables
stars: oscillations *(including pulsations)*
stars: peculiar *(except chemically peculiar)*
(stars:) planetary systems
stars: Population II
stars: Population III
stars: pre-main-sequence
stars: protostars
(stars:) pulsars: general
(stars:) **pulsars: individual: . . .**
stars: rotation
stars: solar-type
(stars:) starspots
stars: statistics
(stars:) subdwarfs
(stars:) supergiants
(stars:) supernovae: general
(stars:) **supernovae: individual: . . .**
stars: variables: Cepheids
stars: variables: Scuti
stars: variables: general
stars: variables: RR Lyrae
stars: variables: S Doradus
stars: variables: T Tauri, Herbig Ae/Be
(stars:) white dwarfs
stars: winds, outflows
stars: Wolf–Rayet

Interstellar medium (ISM), nebulae
ISM: abundances
ISM: atoms
ISM: bubbles
ISM: clouds
(ISM:) cosmic rays
(ISM:) dust, extinction
ISM: evolution
ISM: general
(ISM:) HII regions
(ISM:) Herbig–Haro objects

ISM: individual objects: . . .
(except planetary nebulae)
ISM: jets and outflows
ISM: kinematics and dynamics
ISM: lines and bands
ISM: magnetic fields
ISM: molecules
(ISM:) photodissociation region (PDR)
(ISM:) planetary nebulae: general
(ISM:) **planetary nebulae: individual: . . .**
ISM: structure
ISM: supernova remnants

The Galaxy
Galaxy: abundances
Galaxy: bulge
Galaxy: centre
Galaxy: disc
Galaxy: evolution
Galaxy: formation
Galaxy: fundamental parameters
Galaxy: general
(Galaxy:) globular clusters: general
(Galaxy:) **globular clusters: individual: . . .**
Galaxy: halo
Galaxy: kinematics and dynamics
(Galaxy:) local interstellar matter
Galaxy: nucleus
(Galaxy:) open clusters and associations: general
(Galaxy:) **open clusters and associations: individual: . . .**
(Galaxy:) solar neighbourhood
Galaxy: stellar content
Galaxy: structure

Galaxies
galaxies: abundances
galaxies: active
galaxies: bar
(galaxies:) BL Lacertae objects: general
(galaxies:) **BL Lacertae objects: individual: . . .**
galaxies: bulges
galaxies: clusters: general

galaxies: clusters: individual: . . .
galaxies: clusters: intracluster medium
galaxies: disc
galaxies: distances and redshifts
galaxies: dwarf
galaxies: elliptical and lenticular, cD
galaxies: evolution
galaxies: formation
galaxies: fundamental parameters
galaxies: general
galaxies: groups: general

galaxies: groups: individual: . . .
galaxies: haloes
galaxies: high-redshift

galaxies: individual: . . .
galaxies: interactions
(galaxies:) intergalactic medium
galaxies: irregular
galaxies: ISM
galaxies: jets
galaxies: kinematics and dynamics
(galaxies:) Local Group
galaxies: luminosity function, mass function
(galaxies:) Magellanic Clouds
galaxies: magnetic fields
galaxies: nuclei
galaxies: peculiar
galaxies: photometry
(galaxies:) quasars: absorption lines
(galaxies:) quasars: emission lines
(galaxies:) quasars: general

(galaxies:) **quasars: individual: . . .**
(galaxies:) quasars: supermassive black holes
galaxies: Seyfert
galaxies: spiral
galaxies: starburst
galaxies: star clusters: general

galaxies: star clusters: individual: . . .
galaxies: star formation
galaxies: statistics
galaxies: stellar content
galaxies: structure

Cosmology
(cosmology:) cosmic background radiation
(cosmology:) cosmological parameters
(cosmology:) dark ages, reionization, first stars
(cosmology:) dark energy
(cosmology:) dark matter
(cosmology:) diffuse radiation
(cosmology:) distance scale
(cosmology:) early Universe
(cosmology:) inflation
(cosmology:) large-scale structure of Universe
cosmology: miscellaneous
cosmology: observations
(cosmology:) primordial nucleosynthesis
cosmology: theory

Resolved and unresolved sources as a function of wavelength
gamma-rays: diffuse background
gamma-rays: galaxies
gamma-rays: galaxies: clusters
gamma-rays: general
gamma-rays: ISM
gamma-rays: stars
infrared: diffuse background
infrared: galaxies
infrared: general
infrared: ISM
infrared: planetary systems
infrared: stars
radio continuum: galaxies
radio continuum: general
radio continuum: ISM
radio continuum: planetary systems
radio continuum: stars
radio continuum: transients
radio lines: galaxies
radio lines: general
radio lines: ISM
radio lines: planetary systems
radio lines: stars
submillimetre: diffuse background
submillimetre: galaxies
submillimetre: general
submillimetre: ISM
submillimetre: planetary systems
submillimetre: stars
ultraviolet: galaxies
ultraviolet: general
ultraviolet: ISM
ultraviolet: planetary systems
ultraviolet: stars
X-rays: binaries
X-rays: bursts
X-rays: diffuse background
X-rays: galaxies
X-rays: galaxies: clusters
X-rays: general
X-rays: individual: . . .
X-rays: ISM
X-rays: stars

Transients
(transients:) black hole mergers
(transients:) black hole - neutron star mergers
(transients:) fast radio bursts
(transients:) gamma-ray bursts
(transients:) neutron star mergers
transients: novae
transients: supernovae
transients: tidal disruption events